Article

Cell Reports

Matrix Remodeling Promotes Pulmonary Hypertension through Feedback Mechanoactivation of the YAP/TAZ-miR-130/301 Circuit

Graphical Abstract

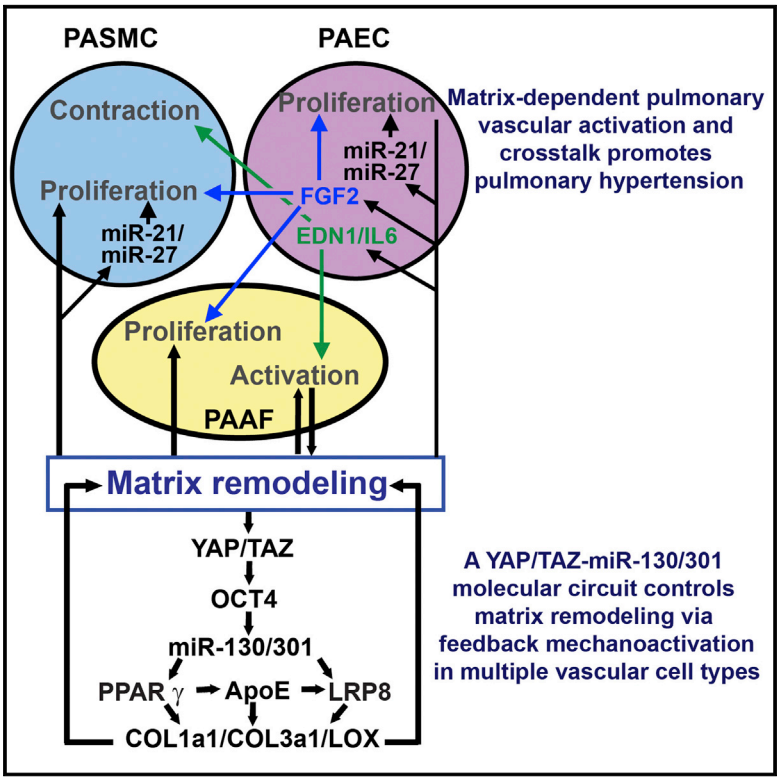

Highlights

- Matrix remodeling induces YAP/TAZ-miR-130/301 early in pulmonary hypertension (PH)
- YAP/TAZ-miR-130/301 promotes matrix remodeling via a mechanoactive feedback loop
- Such matrix remodeling drives pulmonary vascular activation and cellular crosstalk
- Pharmacologic modulation of this circuit ameliorates matrix remodeling and PH

Authors

Thomas Bertero, Katherine A. Cottrill, Yu Lu, ..., B. Nelson Chau, Laura E. Fredenburgh, Stephen Y. Chan

Correspondence

chansy@pitt.edu

In Brief

Bertero et al. establish vascular matrix remodeling as an early, pervasive driver of pulmonary hypertension (PH) controlled by mechanoactive feedback from YAP/TAZ-microRNA-130/301 in multiple cell types. Inhibition of this circuit ameliorated matrix remodeling and PH, thus introducing promising cooperative therapies to treat this disease.

Accession Numbers

GSE61828

Bertero et al., 2015, Cell Reports *13*, 1016–1032
November 3, 2015 ©2015 The Authors
http://dx.doi.org/10.1016/j.celrep.2015.09.049

OPEN ACCESS
CellPress

Cell Reports
Article

Matrix Remodeling Promotes Pulmonary Hypertension through Feedback Mechanoactivation of the YAP/TAZ-miR-130/301 Circuit

Thomas Bertero,[1,11] Katherine A. Cottrill,[1] Yu Lu,[1] Christina M. Haeger,[2] Paul Dieffenbach,[2] Sofia Annis,[1] Andrew Hale,[1] Balkrishen Bhat,[3,12] Vivek Kaimal,[3] Ying-Yi Zhang,[1] Brian B. Graham,[4] Rahul Kumar,[4] Rajan Saggar,[5] Rajeev Saggar,[6] W. Dean Wallace,[5] David J. Ross,[5] Stephen M. Black,[7] Sohrab Fratz,[8] Jeffrey R. Fineman,[9] Sara O. Vargas,[10] Kathleen J. Haley,[2] Aaron B. Waxman,[2] B. Nelson Chau,[3,12] Laura E. Fredenburgh,[2] and Stephen Y. Chan[1,13,*]

[1]Divisions of Cardiovascular and Network Medicine

[2]Division of Pulmonary and Critical Care Medicine

Department of Medicine, Brigham and Women's Hospital, Harvard Medical School, Boston, MA 02115, USA

[3]Regulus Therapeutics, San Diego, CA 92121, USA

[4]Program in Translational Lung Research, University of Colorado, Denver, Aurora, CO 80045, USA

[5]Departments of Medicine and Pathology, David Geffen School of Medicine, University of California, Los Angeles, Los Angeles, CA 90095, USA

[6]Department of Medicine, University of Arizona, Phoenix, AZ 85006, USA

[7]Department of Medicine, University of Arizona, Tuscon, AZ 85724, USA

[8]Department of Pediatric Cardiology and Congenital Heart Disease, DeutschesHerzzentrum München, Klinik an der Technischen Universität München, 80636 Munich, Germany

[9]Department of Pediatrics, Cardiovascular Research Institute, University of California, San Francisco, San Francisco, CA 94131, USA

[10]Department of Pathology, Boston Children's Hospital, Boston, MA 02115, USA

[11]Present address: Institute for Research on Cancer and Aging, University of Nice Sophia Antipolis, 06107 Nice, France

[12]Present address: RaNA Therapeutics, Cambridge, MA 02139, USA

[13]Present address: Pittsburgh Heart, Lung and Blood Vascular Medicine Institute, University of Pittsburgh Medical Center, Pittsburgh, PA 15261, USA

*Correspondence: chansy@pitt.edu

http://dx.doi.org/10.1016/j.celrep.2015.09.049

SUMMARY

Pulmonary hypertension (PH) is a deadly vascular disease with enigmatic molecular origins. We found that vascular extracellular matrix (ECM) remodeling and stiffening are early and pervasive processes that promote PH. In multiple pulmonary vascular cell types, such ECM stiffening induced the microRNA-130/301 family via activation of the co-transcription factors YAP and TAZ. MicroRNA-130/301 controlled a PPARγ-APOE-LRP8 axis, promoting collagen deposition and LOX-dependent remodeling and further upregulating YAP/TAZ via a mechanoactive feedback loop. In turn, ECM remodeling controlled pulmonary vascular cell crosstalk via such mechanotransduction, modulation of secreted vasoactive effectors, and regulation of associated microRNA pathways. In vivo, pharmacologic inhibition of microRNA-130/301, APOE, or LOX activity ameliorated ECM remodeling and PH. Thus, ECM remodeling, as controlled by the YAP/TAZ-miR-130/301 feedback circuit, is an early PH trigger and offers combinatorial therapeutic targets for this devastating disease.

INTRODUCTION

Pulmonary hypertension (PH) is a deadly vascular disease of increasing prevalence worldwide (Chan and Loscalzo, 2008). PH can be induced by myriad triggers, and a growing number of molecular pathways as well as pathogenic crosstalk between pulmonary vascular cell types have been described to influence PH. A majority of the molecular targets chosen for clinical testing primarily affect end-stage disease phenotypes (Boutet et al., 2008; Stenmark and Rabinovitch, 2010). However, they fail to target the enigmatic origins active at early disease time points and thus neither reverse nor prevent PH.

Aberrant collagen and elastin expression (Mecham et al., 1987; Poiani et al., 1990) in the vascular extracellular matrix (ECM) at end-stage PH has long been recognized. Vascular stiffness in the proximal and distal pulmonary arterial tree occurs in various forms of PH (Lammers et al., 2012; Wang and Chesler, 2011), and stiffness is an index of disease progression (Gan et al., 2007). Discrete pharmacologic manipulation of vascular ECM can ameliorate disease (Cowan et al., 2000; Kerr et al., 1984, 1987; Nave et al., 2014). Yet, deeper molecular insights into the causative relationship between vascular ECM remodeling and PH are only just emerging, both at earlier time points of disease and end stage. In general, ECM remodeling is a complex process, occurring through changes in the balance between collagen and elastin deposition, matrix degradation, and matrix remodeling via

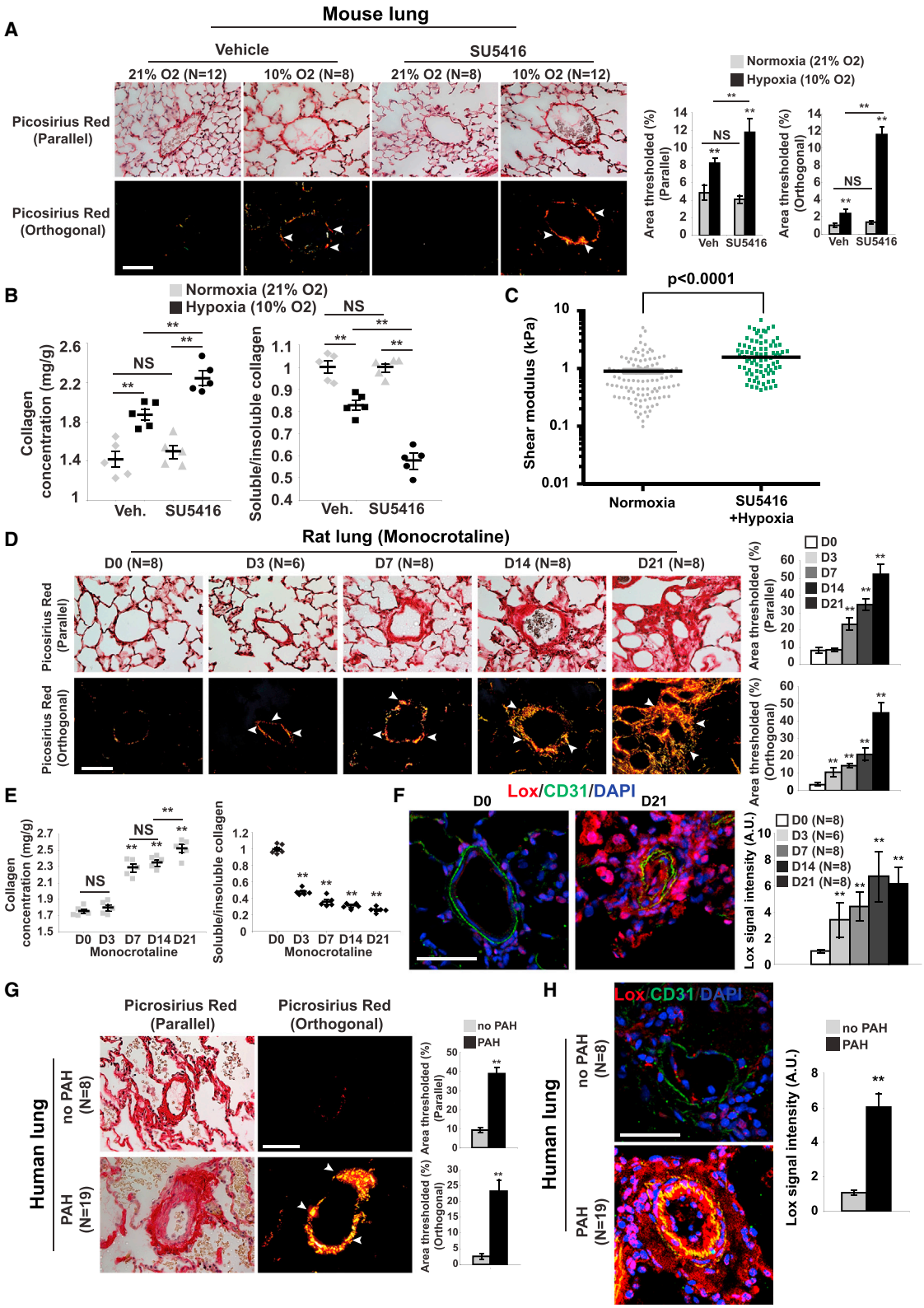

Figure 1. Pulmonary Arteriolar ECM Remodeling and Stiffening Is an Early Hallmark of PH

(A–C) Mice were exposed to hypoxia ± SU5416 (10% O_2 for 3 weeks) in order to induce PH. (A) Picrosirius Red staining of mouse lung tissues was imaged in parallel light to display total collagen content (top) or orthogonal light to display fibrillar collagen (bottom) (<100 μm vessel diameter; 10 vessels/animal). (B)

(legend continued on next page)

collagen crosslinking enzymes such as lysyl oxidase (LOX) (Dufort et al., 2011). In that context of matrix remodeling, two related transcriptional coactivators, YAP (Yes-associated protein 1) and TAZ (transcriptional coactivator with PDZ-binding motif), are crucial for mechanotransduction, a process that converts extracellular mechanical cues into intracellular signaling (Dupont et al., 2011; Piccolo et al., 2014) and is known to regulate cellular proliferation, survival, polarity, organ size, and the ECM, particularly in development and cancer progression. More recently, YAP/TAZ have been implicated in vascular development (Zhou, 2014) and pulmonary parenchymal fibrosis (Liu et al., 2015). However, two key concepts remain undefined: (1) the mechanosensitive pathways that regulate ECM remodeling, particularly in the pulmonary vasculature; and (2) their exact relation to PH.

MicroRNAs (miRNAs) are essential mediators of multiple cellular processes involving cell-cell and cell-matrix interactions (Valastyan and Weinberg, 2011). Yet, we have little prior knowledge regarding the biomechanical effects of ECM on any noncoding RNAs, beyond special contexts of cancer (Mouw et al., 2014). Furthermore, crosstalk among miRNAs, the ECM, and downstream pulmonary vascular phenotypes has been largely unexplored. Previously, we described the proliferative and vasoconstrictive actions of miR-130/301 in PH (Bertero et al., 2014, 2015). Yet, beyond these functions, we have now found a prominent component of their related gene targets associated with ECM biology. Therefore, in this study, we interrogated whether arteriolar ECM modification is an early driver of PH progression, regulated by a complex network of mechanosensitive factors involving miR-130/301.

RESULTS

PH Is Characterized by a Programmatic Shift in Fibrotic Gene Expression with Early and Sustained Arteriolar Collagen Remodeling

To characterize initially the relevance of ECM biology in PH, we performed a transcriptomic analysis of PH lung tissue from mice (chronic hypoxia with administration of the VEGF receptor antagonist SU5416) (Ciuclan et al., 2011). RNA sequencing coupled with pathway enrichment revealed dysregulated genes involved in ECM plasticity specifically (index pathway #4 ECM organization, #7 ECM receptor interaction; Table S1) as well as pathways indirectly associated with ECM stiffening and the collagen crosslinking enzyme LOX (index #1 and #18; Table S1). As a result, such mice displayed increased pulmonary collagen content and fibrillar collagen, as reflected by in situ Picrosirius Red stain (Figure 1A), collagen isoform and LOX transcript analysis (Figure S1A), Lox-dependent collagen crosslinking activity (Figure S1B), and biochemical analysis of pulmonary collagen content (Figure 1B). In correlation, atomic force microscopy revealed an increase in pulmonary arteriolar stiffness in PH mice (Figure 1C). In a separate animal model, PH induced by monocrotaline exposure in rats led to similar increases in pulmonary vascular collagen content (total and fibrillar) (Figures 1D and 1E; Figures S1C and S1D). Of note, Lox expression was increased throughout the PH arteriolar wall, evident in the intimal, medial, and adventitial layers (Figure 1F) and generally consistent with the location of fibrillar collagen (Figure 1D, particularly day 21 of disease). Moreover, in monocrotaline-induced PH in rats, the early phases of PH development (3 days post-monocrotaline exposure) were characterized by increased arteriolar fibrillar collagen (Figures 1D and 1E) and Lox activity (Figure S1D) prior to hemodynamic PH manifestation (as assessed by right ventricular systolic pressure [RVSP]) (Figure S1E) or increased medial thickening (Figure S1F). To prove the relevance of these findings across various forms of PH, six additional animal models of hemodynamically confirmed PH (RVSP measurements; data not shown) also displayed evidence of alterations in pulmonary vascular ECM remodeling, including hypoxia-driven models such as mice exposed to chronic hypoxia alone (Figures S1A and S1B), rats exposed to chronic hypoxia + SU5416 (Figure S1G), and *VHL* null mice (Figures S1H and S1I); inflammatory-driven models such as mice expressing transgenic IL-6 (Figures S1J and S1K) and *Schistosoma mansoni*–infected mice (Figures S1L and S1M); and a surgical lamb model of congenital heart disease (Figure S1N). Finally, similar vascular ECM remodeling and Lox upregulation were observed in human pulmonary arterial hypertension (PAH) tissue (cohorts described in Bertero et al., 2014; Figures 1G and 1H). Together, these results demonstrate that arteriolar ECM stiffening is an early and pervasive process in PH and is associated with a *programmatic* shift in a network of ECM-related genes.

ECM Stiffness Is a Mechanical Stimulus for miR-130/301 Family Expression via YAP/TAZ Signaling

Among the predicted pool of target genes for the PH-associated miR-130/301 family (miR-130a/b; miR-301a/b, and miR-454), we observed a broad component of factors related to ECM remodeling (Figure 2A, encircled genes). To delineate further the connections among this miRNA family, the ECM, and PH, we constructed in silico a "fibrosis network" based on curated seed genes known to be *causatively* involved in ECM remodeling (Table S2) and their first-degree interactors (Table S3). The final fibrosis network (Figure 2A; Table S3) displayed substantial identity (Figure 2A,

Increased total collagen and fibrillar collagen (decreased soluble/insoluble ratio) in PH lung were demonstrated by Sircol assay. (C) Atomic force microscopy revealed increased pulmonary arteriolar (<50 μm) stiffness in PH lung (n = 3 mice) versus untreated (n = 4 mice); horizontal lines denotes median; symbols denote individual PA measurements. p value calculated by Mann Whitney *U* test.

(D–F) Monocrotaline was administered to rats (3 weeks, n = 6–8/time point) to induce PH. Picrosirius Red staining (D) and Sircol assay (E) revealed increased arteriolar fibrillar collagen (starting at D3) evident prior to hemodynamic disease (see Figure S1K). Increased Lox in intimal and media of rat PH pulmonary arterioles was demonstrated by immunofluorescence (F).

(G) Using Picrosirius Red staining of human lung, quantification of <200 μm vessels (10 vessels/patient) revealed increased collagen deposition and fibrillar collagen expression in PAH.

(H) Lox was increased in intima and media of human PAH lung arterioles, shown by immunofluorescence.

Data are expressed as mean ± SEM (*p < 0.05; **p < 0.01, ***p < 0.001, ****p < 0.0001). Scale bars, 50 μm. See also Figure S1.

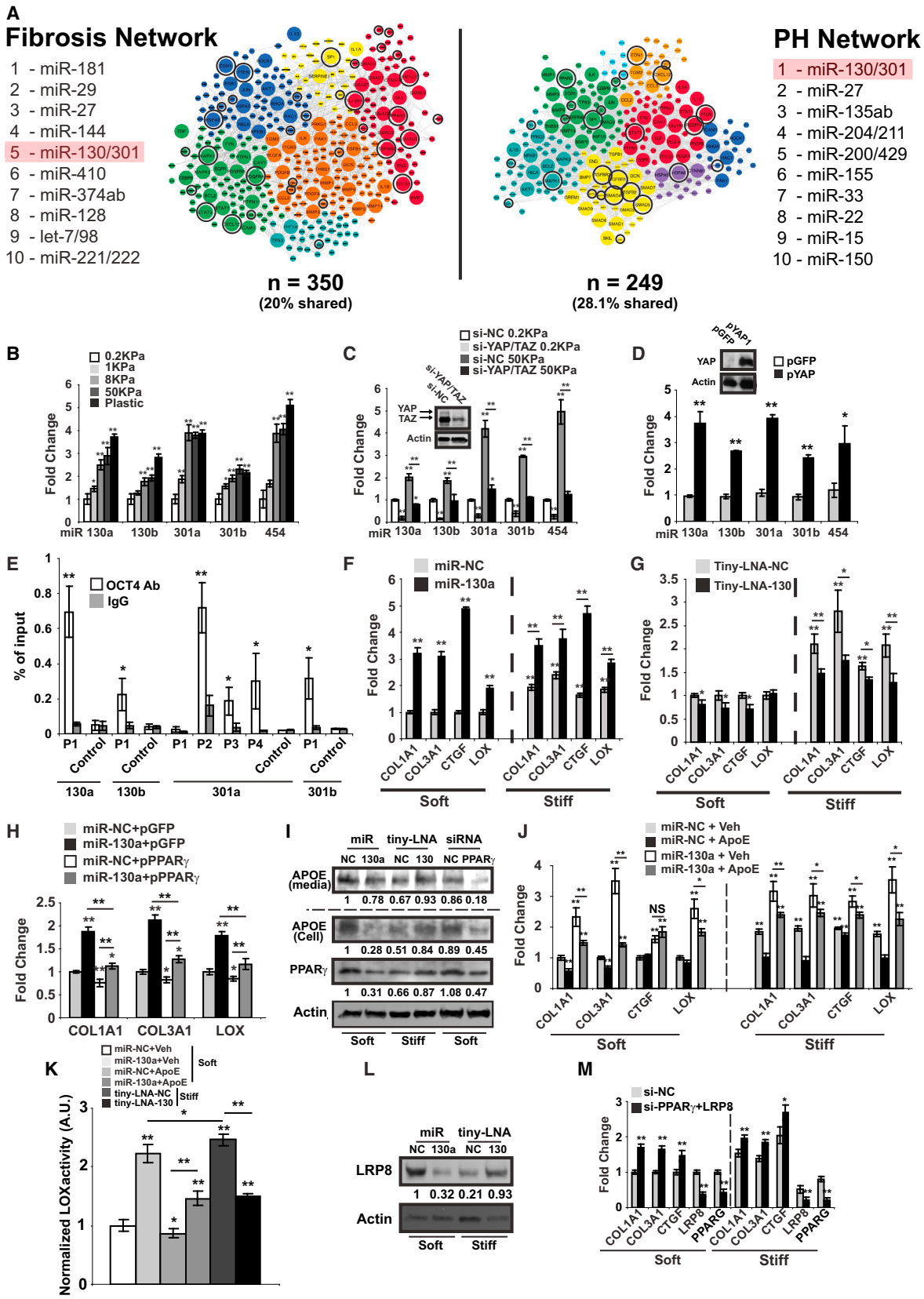

(legend on next page)

encircled and enlarged genes) with the similarly curated and previously described PH gene network (Bertero et al., 2014). Furthermore, miR-130/301 members were highly ranked (#5 among all conserved miRNAs in TargetScan 6.2) by "miRNA spanning score" (based on number and architectural distribution of predicted miRNA targets; see Experimental Procedures), thus indicating their control over multiple pathways in the fibrosis network (Figure 2A; Table S4). Thus, as predicted by network analysis, the miR-130/301 family carries both overlapping and systems-wide effects in both the PH and fibrosis networks.

To begin to evaluate the connection of miR-130/301 to the ECM, we found that miR-130/301 members were upregulated in pulmonary arterial adventitial fibroblasts (PAAFs) after culture in hydrogels of increasing stiffness (Figure 2B). Stiff matrix also upregulated YAP in PAAFs (Figure S2A) without concomitant alterations of total or phosphorylated forms of the LATS or MST1/2 kinases, factors previously linked to YAP activation (Piccolo et al., 2014). Nonetheless, given the known link between mechanotransduction and YAP/TAZ (Dupont et al., 2011), we postulated that YAP and TAZ may control the downstream miR-130/301 mechanosensitive response. Only small interfering RNA (siRNA) knockdown of YAP and TAZ together (Figure 2C), but not separately (Figures S2B–S2D), reversed miR-130/301 upregulation, indicating the dependence upon coordinated activation of YAP/TAZ. Conversely, forced expression of YAP in PAAFs was sufficient to induce miR-130/301 (Figure 2D). No YAP/TAZ-specific TEAD binding site was predicted in the promoter regions of these miRNAs. Instead, we postulated that YAP/TAZ may induce miR-130/301 via increase of the transcription factor POU5F1/OCT4, a target of YAP/TAZ (Lian et al., 2010) and a factor that upregulates miR-130/301 in hypoxia (Bertero et al., 2014). To address definitively the mechanism of regulation of miR-130/301 by POU5F1/OCT4, chromatin immunoprecipitation (ChIP) qPCR demonstrated active OCT4 binding sites in distinct promoter regions of the miR-130/301 genomic loci (Figure 2E). In correlation, POU5F1/OCT4 was induced by matrix stiffness in PAAFs and reversed by YAP/TAZ knockdown (Figure S2E). Additionally, knockdown of POU5F1/OCT4 (Figure S2F) reversed miR-130/301 mechanoinduction (Figure S2G) as well as reversed induction of miR-130/301 by YAP overexpression (data not shown). Similar findings were observed in other pulmonary vascular cell types (Figures S2H–S2M). Together, these results indicate that, across cell types, coordinated upregulation of the miR-130/301 family by mechanical ECM remodeling is mediated by a unique YAP/TAZ- and POU5F1/OCT4-dependent pathway.

The miR-130/301 Family Controls a Cohort of Factors Relevant to Fibrosis in the Lung

Downstream of YAP/TAZ, we examined the consequent effects of miR-130/301 on known fibrotic factors within the lung as well as biochemical properties of the ECM. In cultured PAAFs, either forced miR-130a expression or high ECM stiffness increased transcripts encoding fibrillar collagen isoforms, LOX, and CTGF, a direct target of YAP/TAZ (Dupont et al., 2011) and marker of ECM stiffening and fibrosis (Figure 2F), as well as increased collagen production (Figure S3A). Similar findings were observed in other pulmonary vascular cell types (Figures S3B–S3D). Conversely, in high ECM stiffness, short locked nucleic acid inhibitory oligonucleotides ("tiny-LNAs") with antisense complementarity to the miR-130/301 seed sequence (tiny-LNA-130) decreased transcript expression of this fibrotic gene cohort (Figure 2G) and decreased collagen production (Figure S3A). Thus, these results define miR-130/301 as a broad molecular regulator of ECM modification.

miR-130/301 Controls Collagen Deposition and Remodeling via the PPARγ-APOE-LRP8 Axis

To elucidate molecular factors facilitating collagen deposition and remodeling downstream of miR-130/301, we studied

Figure 2. ECM Stiffening Induces miR-130/301 for Downstream Modulation of Collagen Deposition and Remodeling through a PPARγ-ApoE-LRP8 Axis

(A) A fibrosis network, composed of known fibrotic genes and their closest first-degree interactors (left, Tables S2 and S3), shares a large portion of its members with a PH disease network (right, as previously described; Bertero et al., 2014). Color-coding denotes architectural network clusters. Enlarged nodes are shared by both networks (70 nodes), and encircled genes are miR-130/301 direct targets (per Targetscan 6.2), thus highlighting a prominent fibrotic component among the miR-130/301 targets. miR-130/301 was ranked among the top five miRNA by "spanning score" (Bertero et al., 2014) in both network contexts, reflecting the functional overlap and this miRNA family's shared, systems-level control over both networks.

(B and C) miR-130/301 expression was quantified in human PAAFs cultured in hydrogel of varying stiffness (B) and transfected with siRNAs (YAP/TAZ versus si-NC control) (C).

(D) miR-130/301 was increased in human PAAFs overexpressing YAP (pYAP) versus a control vector (pGFP).

(E) ChIP-qPCR confirmed the presence of OCT4 binding sites (P1–P4) in distinct miR-130/301 family member promoter regions near the transcription start site (proximal promoter 1Kb). Results are expressed as percent of total input DNA prior to immunoprecipitation.

(F and G) PAAFs were transfected with miR-NC, miR-130a, tiny-LNA-NC, or tiny-LNA-130 and cultivated in soft or stiff matrix. Forced miR-130a expression or stiff matrix increased collagen transcripts, LOX, and CTGF, a marker of ECM stiffening and fibrosis (F). In high ECM stiffness, tiny-LNA-130 decreased this fibrotic gene cohort (G).

(H) By qRT-PCR in PAAFs, constitutive PPARγ (pPPARγ) reversed the miR-130a-induced upregulation of collagen and LOX.

(I) By immunoblot, miR-130a, matrix stiffening, and PPARγ knockdown decreased ApoE while inhibition of miR-130/301 (tiny-LNA-130) increased ApoE in stiff conditions.

(J) PAAFs exposed to exogenous ApoE were resistant to miR-130a-induced upregulation of collagen, CTGF, and LOX.

(K) Lox activity was measured in PAAFs cultured in soft or stiff matrix and treated with miR-130a ± exogenous ApoE or miR-130/301 inhibitor (tiny-LNA-130).

(L) By immunoblot, LRP8 was reduced by miR-130a or matrix stiffening and preserved by miR-130/301 inhibition.

(M) siRNA knockdown of both LRP8 and PPARγ increased collagen and CTGF.

In all panels, mean expression in control groups (0.2 KPa, miR-NC, tiny-LNA-NC, or si-NC in soft matrix) was assigned a fold change of 1, to which relevant samples were compared. Data are expressed as mean ± SD (*$p < 0.05$; **$p < 0.01$). See also Figures S2 and S3.

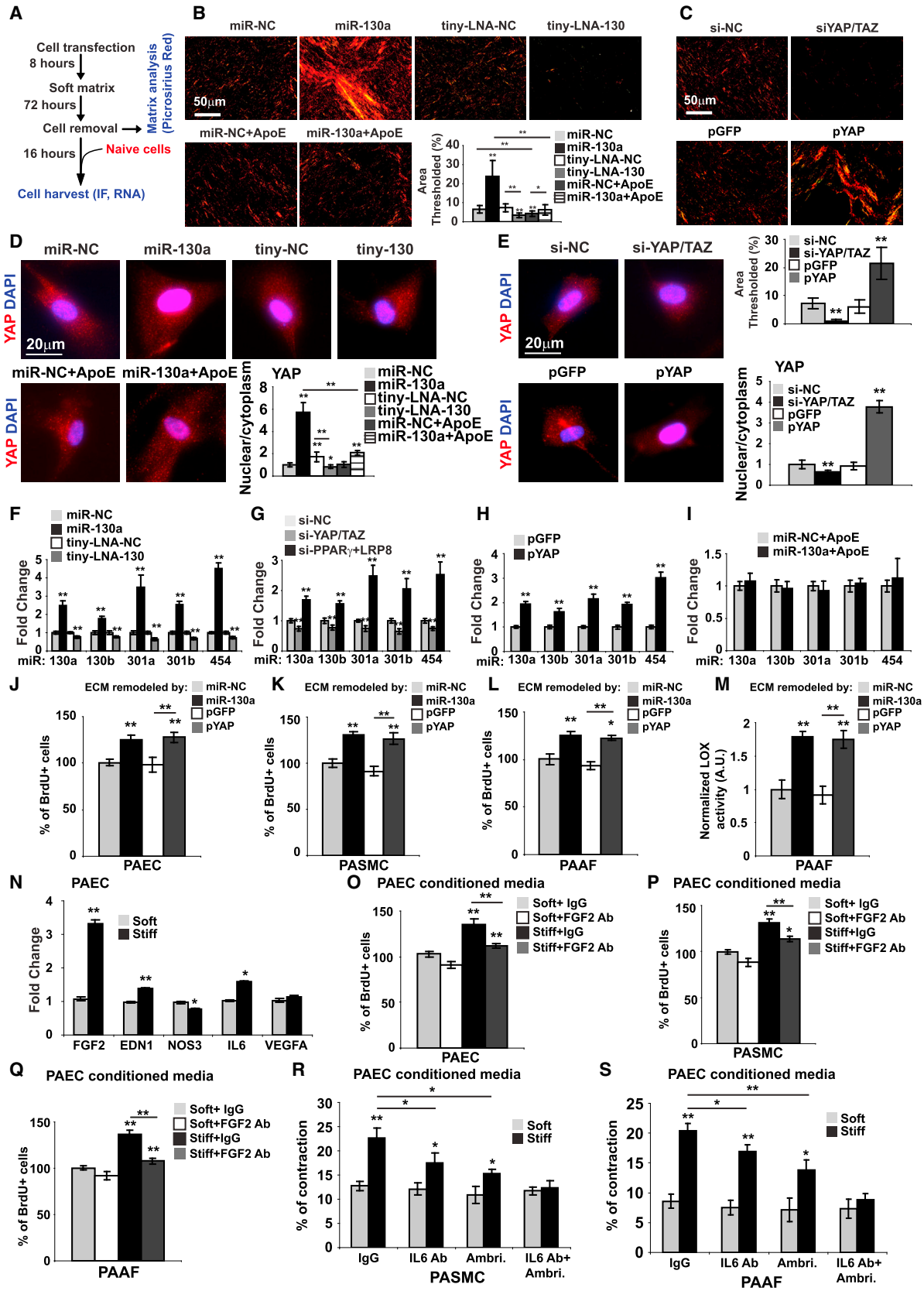

(legend on next page)

peroxisome proliferator-activated receptor gamma (PPARγ), a known target of miR-130/301 in control of cellular proliferation (Bertero et al., 2014) with a known role in ECM modification in other contexts (Wei et al., 2012). Constitutive PPARγ disrupted the miR-130/301-mediated upregulation of collagen and LOX in PAAFs (Figure 2H). Notably, miR-130a overexpression or PPARγ knockdown (Figure 2I) decreased apolipoprotein E (ApoE), a direct target of PPARγ (Hansmann et al., 2008) involved in ECM remodeling (Kothapalli et al., 2012). In contrast, miR-130/301 inhibition in stiff ECM increased ApoE (Figure 2I), and PAAFs exposed to media enriched with ApoE were similarly resistant to miR-130/301 activity (Figures 2J and 2K). Downstream of PPARγ and ApoE, PPARγ knockdown alone in soft conditions increased the aforementioned cohort of fibrotic genes (Figure S3E). Conversely, constitutive PPARγ expression (pPPARγ) or ApoE treatment disrupted the miR-130/301-mediated upregulation of collagen production (Figure S3F) and the miR-130/301-mediated upregulation of Lox activity (Figure 2K). Of note, the regulation of Lox activity by miR-130/301 corresponded with consistent alterations of expression of cleaved, activated Lox in these cultured PAAFs (data not shown). Thus, the miR-130/301 family critically relies on PPARγ and ApoE to control collagen deposition and remodeling.

Given the role of ApoE and a predicted miR-130/301 binding site in the ApoE receptor LRP8 transcript (TargetScan 6.2; Friedman et al., 2009), we considered that LRP8 may also function prominently here. Using a luciferase reporter assay, we confirmed LRP8 as a direct miR-130/301 target (Figure S3G). In cultured PAAFs, miR-130a decreased LRP8 expression, while inhibition of miR-130/301 increased LRP8 (Figure 2L). As with PPARγ knockdown, LRP8 knockdown increased collagen expression and Lox activity (Figures S3H–S3J). Importantly, knockdown of PPARγ and LRP8 together induced a more robust response than either knockdown alone, indicating their coordinated roles in controlling collagen expression (Figure 2M; Figures S3I and S3J).

Finally, we postulated that miR-130/301 may be central to a feedback loop amplifying fibroblast activation and ECM remodeling in PH. PAAFs were transfected with miR-130a mimic oligonucleotides or siRNAs for PPARγ and LRP8 or infected with a lentivirus carrying a YAP transgene (pYAP) and cultured in soft matrix to remodel the ECM. Cells were then removed from this ECM and replaced with non-transfected, naive PAAFs (Figure 3A; analyses of remodeled ECM in Figures 3B and 3C; Figure S4A). After 16 hr, ECM remodeled by miR-130a or YAP promoted YAP nuclear localization (Figures 3D and 3E; Figure S4B) and increased POU5F1/OCT4 (Figure S4C), miR-130/301 (Figures 3F–3H), and downstream fibrosis-relevant genes (Figures S4C and S4D) in naive PAAFs. Conversely, when ECM remodeling was inhibited by miR-130/301 or YAP/TAZ knockdown, a decrease was observed in YAP nuclear localization (Figures 3D and 3E), POU5F1/OCT4 (Figures S4C and S4E), miR-130/301 (Figures 3F and 3G), and the fibrosis gene cohort (Figure S4E). Importantly, the ECM modifications activating downstream fibrosis-relevant genes and miR-130/301 were reversed by ApoE (Figures 3B, 3D, and 3I; Figure S4F). Taken together, these results reveal that miR-130/301 and YAP/TAZ act in a feedback-driven, self-amplifying regulatory loop that integrates multiple direct target genes including PPARγ and LRP8 in order to regulate coordinately ECM remodeling and stiffening.

miR-130/301-Dependent ECM Remodeling Controls Vascular Cell Proliferation and Pulmonary Vascular Crosstalk

Next, we postulated that miR-130/301-dependent ECM remodeling controls specific downstream molecular functions and PH-relevant cellular phenotypes. ECM remodeled by forced expression of miR-130a or YAP in PAAFs increased proliferation of naive pulmonary artery endothelial cells (PAECs) (Figure 3J) and pulmonary artery smooth muscle cells (PASMCs) (Figure 3K). In naive PAAFs plated in these matrices, ECM modification also upregulated proliferation (Figure 3L) and Lox activity (Figure 3M). Correlating with these findings, in naive PAECs, PASMCs, and PAAFs (Figures S4G–S4J), ECM remodeling induced the expression of miR-21 and miR-27a, miRNAs that are active in controlling pulmonary vascular cell proliferation (Figures S4K–S4M) and previously implicated in PH pathogenesis in vivo (Bi et al., 2015; White et al., 2012). Beyond direct control of proliferation, in PAECs, ECM stiffening induced a panel of secreted vasoactive effectors implicated in PH, including the pro-proliferative cytokine FGF2, the vasoconstrictor EDN1, and the inflammatory cytokine IL-6. ECM remodeling also downregulated endothelial

Figure 3. A YAP/TAZ-miR-130/301 Feedback Loop Promotes ECM Modification to Induce Dysregulated Pulmonary Vascular Crosstalk

(A) Schema of the experimental procedure.

(B) ECM staining by picrosirius red revealed that miR-130a increased fibrillar collagen, while miR-130/301 inhibition (tiny-LNA-130) or ApoE reversed such effects.

(C) Similarly, YAP (pYAP) increased fibrillar collagen as compared with control (pGFP), while knockdown of YAP/TAZ (siYAP/TAZ) decreased fibrillar collagen.

(D and E) In that context, immunofluorescence for YAP (red) and nuclei (DAPI, blue) was performed on naive PAAFs plated on ECM remodeled by the indicated conditions. Nuclear stain relative to cytosolic stain of YAP was quantified (n = 3 experiments with ten 20× fields analyzed per experiment).

(F–H) qRT-PCR revealed that ECM remodeled by miR-130a (F) or by siPPARγ+LRP8 (G) or by YAP (H) upregulated miR-130/301 in naive cells plated on remodeled ECM. Conversely, ECM remodeled by tiny-LNA-130 (F) or si-YAP/TAZ (G) downregulated miR-130/301 in naive cells.

(I) miR-130/301 induction in naive cells cultured on matrix remodeled by miR-130a was reversed by ApoE.

(J–M) Direct cellular effects of miR-130a/YAP-dependent stiffness were demonstrated by increased proliferation (BrdU-staining) of PAECs (J), PASMCs (K), and PAAFs (L) when culturing in ECM remodeled by PAAFs overexpressing miR-130a or YAP. Such ECM also increased LOX activity in PAAFs (M).

(N–S) Pulmonary vascular cell crosstalk dependent on ECM remodeling was revealed by modulation of a panel of vasoactive genes in PAECs via stiff ECM (N). Conditioned media from PAECs cultured in such stiff matrix increased proliferation in naive PAECs (O), PASMCs (P), and PAAFs (Q) and was reversed by a FGF2 blocking antibody (FGF2 Ab). Conditioned media from PAECs cultured in stiff ECM increased contraction of PASMCs (R) and PAAFs (S). Contraction was partially reversed by ambrisentan or an IL-6 antibody (IL6 Ab) alone and more robustly reversed by their combination.

In all panels, mean expression in control groups (miR-NC, tiny-LNA-NC, or si-NC in soft matrix) was assigned a fold change of 1, to which relevant samples were compared. Data are expressed as mean ± SD (*$p < 0.05$; **$p < 0.01$). See also Figure S4.

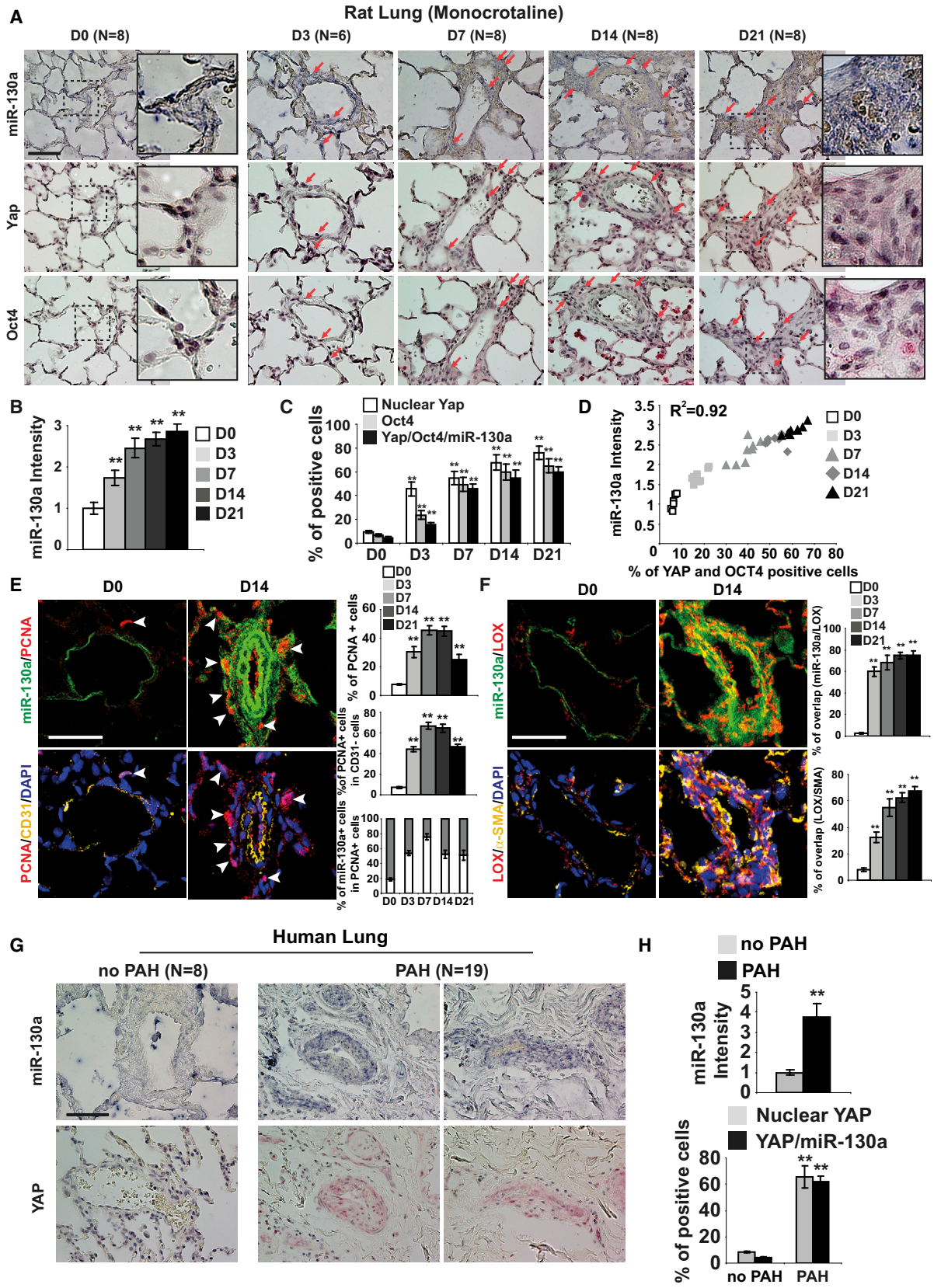

(legend on next page)

nitric oxide synthase NOS3 (Figure 3N). Conditioned media from PAECs cultivated in stiff matrix activated the proliferation of naive PAECs (Figure 3O), PASMCs (Figure 3P) and PAAFs (Figure 3Q); such proliferation was partially reversed by a FGF2 blocking antibody. PAEC-conditioned media also activated PASMC (Figure 3R) and PAAF (Figure 3S) contraction. Implicating END1 and IL-6 as causative factors, contraction was partially reversed by the endothelin receptor antagonist ambrisentan or an IL-6 blocking antibody alone and, to a better extent, by these agents together (Figures 3R and 3S). Thus, the YAP/TAZ miR-130/301 circuit remodels ECM for control of associated miRNA-dependent cellular proliferation as well as pulmonary vascular cell crosstalk related to contractile response.

The YAP/TAZ-miR-130/301 Circuit Promotes Matrix Remodeling and PH In Vivo

We wanted to determine whether the YAP/TAZ-miR-130/301 circuit is active in PH in vivo and correlates with markers of arteriolar ECM remodeling. As PH progressed in monocrotaline-exposed rats (Figures 4A–4F; Figure S5), in situ arteriolar staining displayed a strong positive correlation among YAP, POU5F1/OCT4, and miR-130a expression. By immunofluorescence, miR-130a expression was also associated with increased proliferation (PCNA nuclear stain in multiple vessel layers but particularly in the outer layers; Figure 4E) and increased Lox expression (staining throughout the vessel wall; Figure 4F). Importantly, correlating with early and sustained ECM remodeling (Figures 1D and 1E), staining of all markers was increased at every disease time point, including early D3. Similar increases in YAP and miR-130a were observed in human PH patients (as described in Bertero et al., 2014; Figures 4G and 4H).

To determine whether miR-130a alone promotes vascular matrix remodeling in vivo, miR-130a mimic oligonucleotides were delivered in mice via serial intrapharyngeal delivery. miR-130a reduced target gene expression (i.e., LRP8), increased collagen deposition and remodeling (Figures 5A, 5B, and 5D), and promoted Lox expression and activity (Figures 5B and 5C). Notably, miR-130a exposure was also accompanied by vascular YAP nuclear localization and YAP-dependent gene expression (i.e., CTGF) (Figures 5A and 5B), consistent with our in vitro evidence of a feedback loop between ECM remodeling and endogenous YAP/TAZ-miR-130/301 induction. These events ultimately increased proliferation in both endothelial and smooth muscle compartments (PCNA staining; Figure 5E) and promoted PH (Figures 5F–5H), as reflected by RVSP, right ventricular remodeling (RV/LV+S ratio), and pulmonary arteriolar muscularization. Conversely, experiments were designed to prevent collagen remodeling via serial treatment with a pharmacologic inhibitor of LOX (Levental et al., 2009), β-aminopropionitrile (BAPN). In miR-130-exposed mice, inhibition of LOX by BAPN reversed indices of ECM remodeling (Figures 5A–5D). Consistent with an ECM-YAP feedback loop, BAPN also reversed YAP activation, blunted the ongoing effects of miR-130a on LRP8 repression and collagen deposition and remodeling (Figures 5A and 5B), and ultimately reversed miR-130a-dependent proliferation (Figure 5E) and downstream PH manifestations (Figures 5F–5H). Thus, miR-130a is sufficient to promote pulmonary vascular ECM remodeling in PH and is dependent upon a feedback loop via the ECM and YAP/TAZ.

To determine whether inhibition of miR-130/301 ameliorates vascular ECM remodeling in PH, hypoxia+SU5416-exposed mice and monocrotaline-exposed rats were examined (Figure 6). Rodents were serially administered a "shortmer" oligonucleotide recognizing the miR-130/301 seed sequence (Short-130), thus inhibiting all miR-130/301 members in vivo, as demonstrated in mouse lung (Bertero et al., 2014) and rat lung (Figure S5). In monocrotaline-exposed rats, Short-130 reversed the decrease of the miR-130/301 targets Lrp8 and Pparγ in diseased control pulmonary arterioles (Short-NC) (Figure 6A; Figure S5). This was accompanied by consequent decreases in Lox expression (Figure 6B; Figure S5), Lox activity (Figure 6C), and collagen deposition and fibrillar collagen expression (Figures 6A, 6B, and 6D). Again reflecting the ECM-YAP feedback loop, miR-130/301 inhibition and its effects on ECM remodeling also decreased YAP nuclear localization (Figure 6A) and YAP activation (reflected by decreased Ctgf; Figure 6B). Together, these effects culminated in reduced cellular proliferation (decreased PCNA in intimal and medial vessel layers; Figure 6E) and decreased hemodynamic and histologic severity of PH (Figures 6F and 6G). Similarly, in hypoxia+SU5416-exposed mice, where PH is known to improve with Short-130 treatment (Bertero et al., 2014), miR-130/301 inhibition reversed collagen deposition and fibrillar collagen remodeling (Figure 6H) and blunted hypoxia-induced vascular stiffening, as demonstrated by atomic force microscopy (Figure 6I). Furthermore, although whole-lung transcriptomics likely captured only a subset of the miR-130/301 targets affecting the diseased pulmonary vasculature, such analyses of mouse lung with hypoxia+SU5416-induced PH revealed a generalized de-repression of miR-130/301 targets by Short-130 (data not shown) and a generalized de-repression of hypoxia induced genes (Table S5), many of which overlap with known genes in the fibrosis network and ECM plasticity in general. Pathway enrichment of genes revealed pronounced representation of several pathways known to be involved in fibrosis (Figure 6J; Table S6). Thus, rather than relying on one single gene target or pathway, the miR-130/301 family induces a *programmatic* molecular shift toward the fibrotic pathophenotype in vivo. In sum, miR-130/301 is both necessary and sufficient to promote pulmonary vascular stiffening and consequent PH manifestations.

Figure 4. The YAP/TAZ-miR-130/301 Molecular Circuit Is Active in Rodent and Human Examples of PH

(A–F) Monocrotaline was administered to rats (3 weeks, n = 6–8/time point) to induce PH (see Figure 1). In serial sections of pulmonary arterioles (A), quantification of stain intensity (B) and percentage of positively stained cells (C) revealed a correlation between miR-130a, Yap, and Oct4 expression (D). (E and F) Immunofluorescence stain confirmed an increase of PCNA (E) and Lox (F) expression in miR-130a positive cells.

(G and H) In serial sections of human pulmonary arterioles, a similar relationship was observed between increased miR-130a and YAP in PAH.

Data are expressed as mean ± SD (*$p < 0.05$; **$p < 0.01$). Scale bars, 50 μm. See also Figure S5.

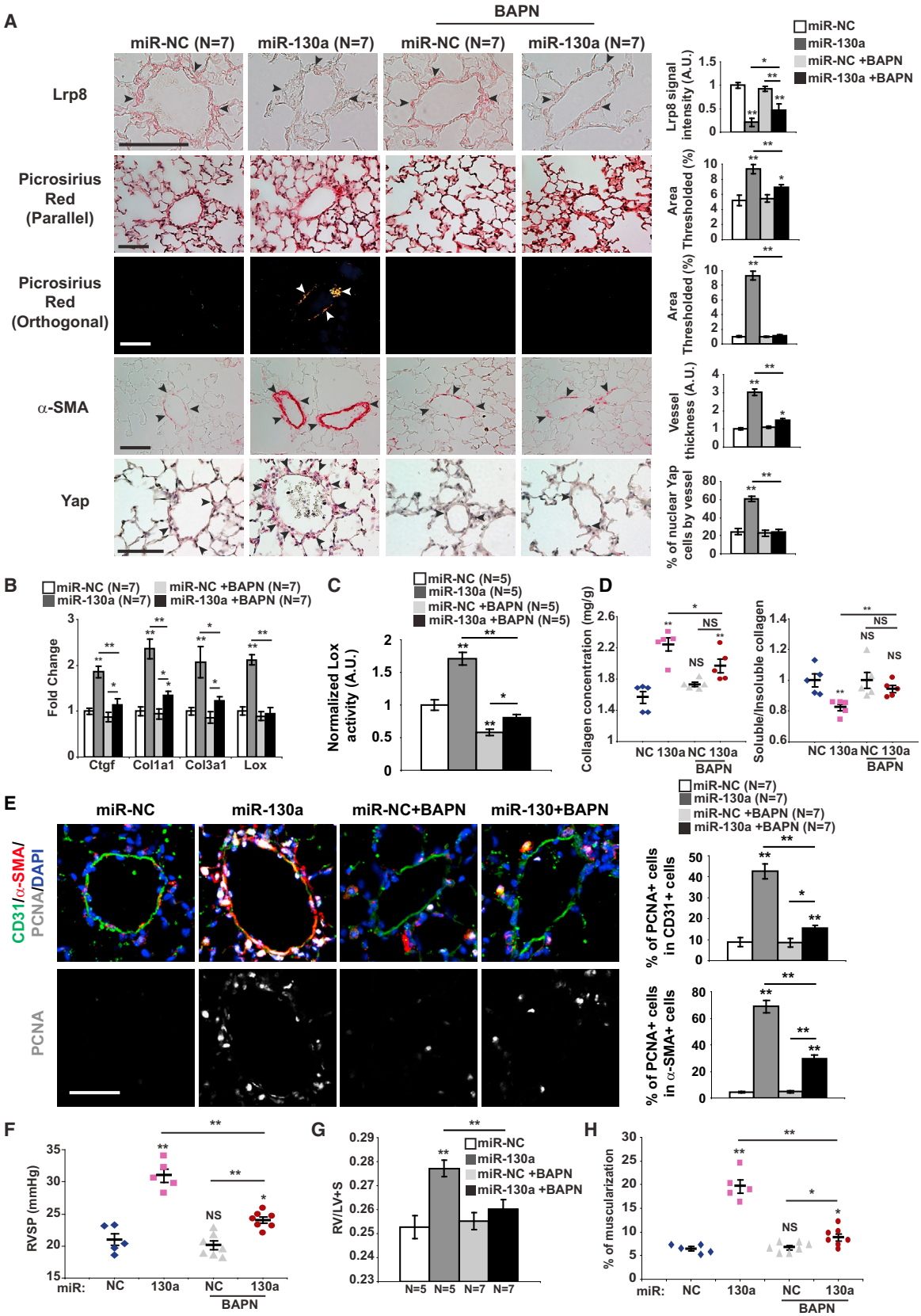

(legend on next page)

Therapeutic Targeting of Downstream ApoE or Lox Reduces ECM Remodeling and Blunts the YAP/TAZ-miR-130/301 Feedback Loop to Ameliorate PH In Vivo

Finally, we wanted to define more definitively the in vivo ECM-YAP/TAZ-miR-130/301 feedback mechanism by pharmacologic manipulation of downstream ECM regulators, ApoE and Lox, in PH. To assess the importance of ApoE activity in PH, mice were treated with daily ingestion of the liver-X nuclear hormone receptor (LXR) agonist GW3965, a pharmacologic inducer of ApoE (Pencheva et al., 2014), simultaneously with hypoxia. Alternatively, similar to experiments with miR-130a-induced PH (Figure 5), BAPN was administered in PH mice either simultaneously with hypoxia ("prevention") or after disease development ("reversal"). In both cases of GW3965 or BAPN treatment, downstream collagen deposition and remodeling (Figures 7A and 7E; Figure S6) as well as Lox expression (Figures 7A and 7E; Figure S6) and activity (Figure 7B,F) were inhibited. In the context of these changes in ECM, GW3965 and BAPN treatment also reduced YAP nuclear localization (Figures 7A and 7E) and activation (reflected by decreased Ctgf; Figure S6), decreased miR-130/301 expression (Figures 7C and 7G), and reversed miR-130/301-dependent Pparγ and Lrp8 downregulation (Figure S6). Consistent with miR-130/301 manipulation in vivo, these feedback events culminated in decreased cellular proliferation in CD31+ and α-SMA+ arteriolar cells (PCNA staining; Figures 7D and 7H) and improved downstream hemodynamic and histologic indices of PH (Figure S6; Figures 7I–7K). Thus, we conclude that the YAP-TAZ-miR-130/301 circuit and its downstream network of targets are programmed to both respond to and promote ECM remodeling in PH and represent an integrally linked set of targets for potential tailored therapy in this disease.

DISCUSSION

Mechanical forces act through a YAP/TAZ-miR-130/301 feedback loop to promote PH via ECM remodeling and vascular stiffening at both early and late time points of disease. In turn, vascular stiffening controls a number of vascular cell phenotypes and crosstalk mechanisms and thus plays a crucial role in PH pathogenesis. This work highlights both the fundamental significance yet complex control of ECM plasticity in PH and the attractive potential of tailoring therapy to this molecular circuit and the related downstream PPARγ-APOE-LRP8-LOX axis.

Previous studies have implicated specific molecules related to the ECM in PH (Merklinger et al., 2005; Nave et al., 2014; Nickel et al., 2015; Wang et al., 2014). Yet, questions persist of whether ECM remodeling is merely an end-stage feature of PH and whether massive fibrosis is necessary to induce pathogenic outcomes. Our work clarifies these points by reporting the early development of ECM remodeling in PH and supporting the notion that dynamic changes of ECM mediated via the YAP/TAZ-miR-130/301 circuit can have relevant pathogenic consequences both early and late in disease. Specifically, in vitro, miR-130/301 members are responsive to modest alterations (1 kPa) of matrix stiffness (Figure 2B; Figures S2H and S2K). Moreover, based on our timed confocal microscopy data, subtle changes in arteriolar stiffening in vivo without massive fibrosis correlate with activation of this pathogenic circuit, particularly at early disease time points (Figure 4; Figure S5). Notably, under conditions where stiffness abates (i.e., transferring cultured cells from stiff to soft matrix), we found downregulation of miR-130/301, suggesting their role as more dynamic mechanical stress response factors in the pulmonary vessel (data not shown). Unlike early-stage disease, control of the YAP/TAZ-miR-130/301 circuit at later disease time points may be much less linear and aligns well with the "multi-hit" hypothesis of the origins of PH (Chan and Loscalzo, 2008). That is, considering that miR-130/301 members are upregulated by stiffness as well as by hypoxia, inflammatory cytokines, and deficiencies of certain factors genetically associated with PH (Bertero et al., 2014, 2015), these effects of disparate disease exposures on YAP/TAZ-miR-130/301, coupled with a potent ECM-YAP/TAZ-positive feedback loop, support a model of self-sustaining and anatomic "spreading" of ECM remodeling as PH progresses. Therefore, it remains an intriguing question as to how and at what time points do other factors and/or diseases clinically associated with PH interface with the YAP/TAZ-miR-130/301 circuitry and ECM biology.

Controlling how cells adapt to their external space (Piccolo et al., 2014), the multi-faceted functionality of YAP/TAZ also sheds light on the interactions of disparate vascular cell types with environmental cues and with each other in PH. Our data indicate that the miRNA-dependent actions of YAP/TAZ are pervasive throughout multiple cell types of the pulmonary vasculature and multiple time points of PH. Such a ubiquitous presence suggests an expansive repertoire of environmental cues that may depend upon these molecules for vascular function, both in health and disease. For example, since shear stress can induce YAP/TAZ (Kim et al., 2014), miR-130/301 may also be responsive to increased pulmonary vascular flow such as in cases of congenital heart disease where PH secondary to shunting predominates. Yet, despite the shared dependence on YAP/TAZ–miR-130/301, downstream events can still be cell-type specific, resulting from the modulation of a cohort of

Figure 5. miR-130a Induces YAP/TAZ-miR-130/301 to Promote Pulmonary Vascular ECM Remodeling in a LOX-Dependent Manner

Along with SU5416, mice received four weekly administrations of miR-NC or miR-130a and were treated either with daily BAPN or vehicle.

(A) In situ staining of mouse lung demonstrated that BAPN blunted miR-130a-specific induction of LRP8, ECM remodeling (Picrosirius Red), and medial thickening (α-SMA), thus leading to decreased YAP nuclear localization.

(B) By qRT-PCR, fibrillar collagen, Lox, and YAP-dependent gene expression (i.e., CTGF), were increased in miR-130a-diseased lung but blunted by BAPN.

(C–E) Lox activity (C), biochemical indices of collagen remodeling (D), and proliferation (PCNA staining in arteriolar CD31$^+$ and α-SMA+ cells) (E) were increased in diseased lung, but blunted by BAPN.

(F–H) BAPN decreased the miR-130-mediated increase in PH severity, as quantified by RVSP (F), Fulton index (RV/LV+S) (G), and pulmonary arteriolar muscularization (H).

Data are expressed as mean ± SEM (*$p < 0.05$; **$p < 0.01$). Normalized values are expressed as arbitrary units (A.U.) in (A) and (C). Scale bars, 50 μm.

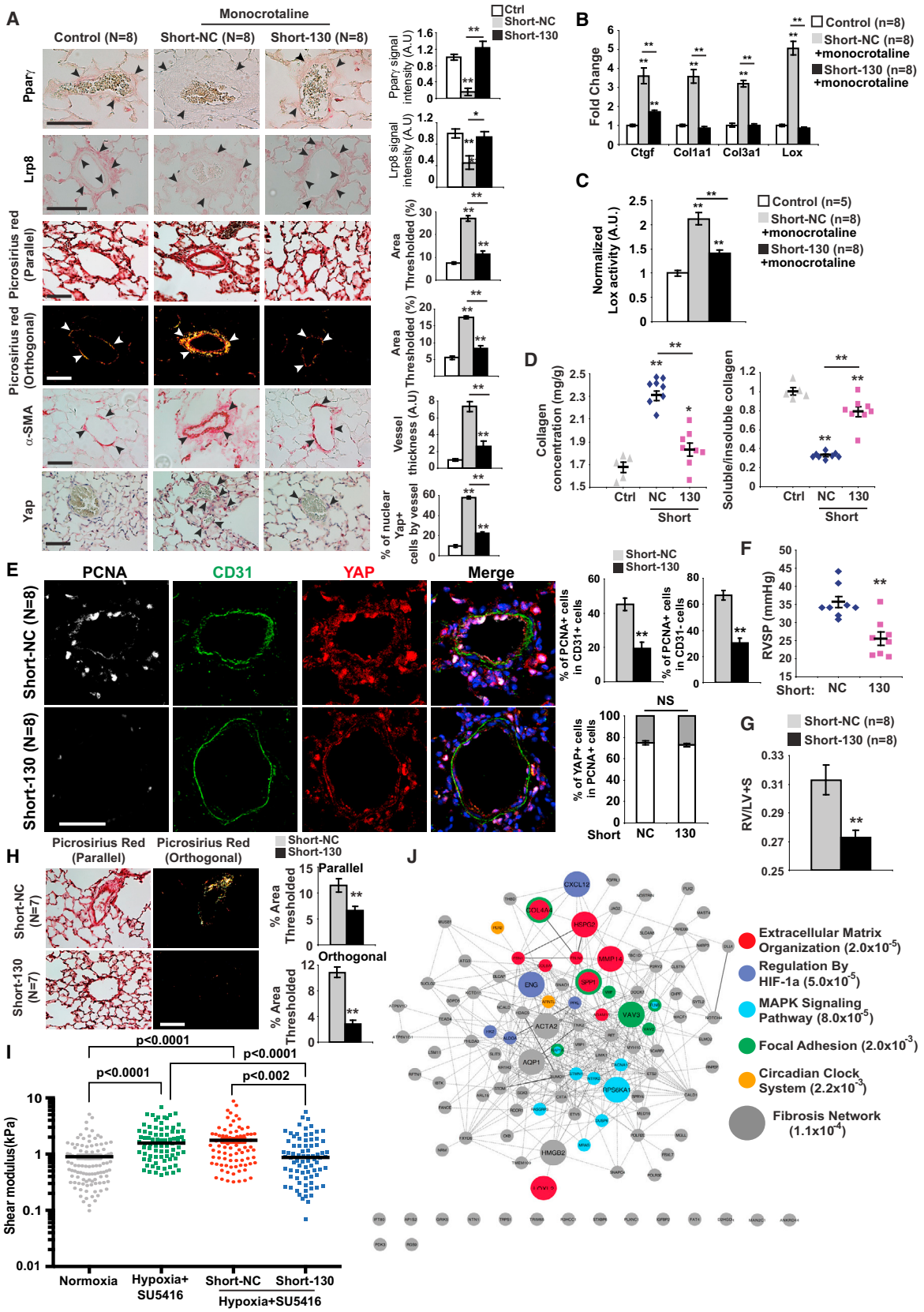

(legend on next page)

downstream pathways and cellular crosstalk patterns, some of which overlap and some of which differ among PAAFs, PAECs, and PASMCs (Figure 3). Considering this degree of specificity and its adjustable, feedback-driven properties, the YAP/TAZ circuit may be partly responsible for individualized "tuning" of ECM remodeling, depending upon each PH subtype or temporal stage. Given such inherent control over the molecular tuning of the vascular ECM, it will be useful in the future to define the pathways beyond LATS and MST1/2 kinase signaling (Figure S2A) that are involved in pulmonary vascular YAP/TAZ mechanoactivation. More generally, it will be intriguing to define the role(s) of the YAP/TAZ-miR-130/301 circuit in other diseased sites throughout the pulmonary vascular tree (Lammers et al., 2012), the peripheral vasculature, and other organ systems plagued by fibrotic states.

Downstream of the YAP/TAZ-miR-130/301 axis, the involvement of the PPARγ-APOE-LRP8-LOX pathway, downstream secreted factors, and additional miRNAs further define the molecular hierarchy and pathway overlap under the control of the ECM. In addition to the relation between the adventitial fibroblast and the vascular ECM, our results describe key molecular signaling pathways that facilitate the direct interplay between the ECM with endothelial and smooth muscle cells as well as the ECM-dependent crosstalk among these cell types. These actions are consistent with previously reported pro-proliferative phenotypes in PH, such as for PPARγ and APOE (Bertero et al., 2014; Hansmann et al., 2008), and consistent with fibrotic phenotypes in other contexts such as for miR-21 (Huang et al., 2015). On the other hand, the regulation of the associated miRNAs miR-21 and miR-27a as well as the vasoactive factors FGF2, IL-6, and EDN1 now better defines the complete cellular pathobiology in PH relevant to ECM remodeling. Much future work remains, as it is likely that an even more complex and wide-reaching interactome exists among YAP/TAZ, miR-130/301, and their targets, all coincident with large portions of the same fibrotic gene network (Figure 2A). As a result, it is possible that other aspects of ECM remodeling such as collagen degradation and turnover may feed into this mechanosensitive miRNA circuit. With such studies, it may be possible to address whether some of these overlapping pathophenotypes linked to YAP/TAZ-miR-130/301 (i.e., fibrosis and proliferation) can be separated from one another during PH and, if so, whether those contexts would result in distinct differences in disease manifestation.

Finally, the paradigm of the YAP/TAZ-miR-130/301 circuit in ECM remodeling may be applied to current suboptimal clinical management in PH. From a diagnostic perspective, it may be feasible to identify new populations at risk for PH via targeted molecular screening of YAP/TAZ or miR-130/301 activity. From a therapeutic perspective, targeting the YAP/TAZ-miR-130/301 circuit and downstream effectors could influence ECM remodeling at both early and late stages of PH, thus presenting an opportunity for disease prevention or reversal. Our findings may also allow for repurposing of a related set of pharmacologic agents in PH, applied previously in unrelated contexts and/or used in isolation rather than coordinated combination. For instance, our data reveal that the LXR agonist GW3965 ameliorates ECM remodeling and PH in vivo (Figure 7; Figure S6). While clinical use of LXR agonists has focused on their roles in lipid and cholesterol metabolism (Im and Osborne, 2011), application of their actions in ECM remodeling beyond cancer metastasis (Pencheva et al., 2014) has yet to be explored. Furthermore, consistent with prior work (Kerr et al., 1984; Nave et al., 2014), our findings demonstrate the utility of LOX inhibition by BAPN for partially ameliorating PH (Figure 7; Figure S6). Importantly, because it inhibits future collagen crosslinks rather than lysing existing ones, BAPN may be inadequate to induce a complete reversal of ECM remodeling; yet, in combination with GW3965, a more robust synergistic effect may be possible. Cyclic YAP-like peptides that interrupt YAP-TEAD interactions in oncogenesis (Zhou et al., 2015) could also carry therapeutic potential in PH. Therefore, when considered with our data demonstrating the efficacy of repressing miR-130/301 via shortmers (Figure 6) and even PPARγ (via rosiglitazone as described in Bertero et al., 2014), these findings suggest that tailored, ECM-based drug combinations may be effective for additive or synergistic control of overall PH manifestation.

In sum, our findings define the central pathogenic importance in PH of the YAP/TAZ-miR-130/301 circuit, at early and late stages of disease, in both responding to and promoting ECM remodeling via the broad control of a fibrotic gene/miRNA network

Figure 6. miR-130/301 Inhibition Disrupts YAP/TAZ-miR-130/301 Signaling and Reverses a Program of ECM Remodeling and PH

(A–G) Following monocrotaline exposure, rats were treated with Short-NC or Short-130. (A) By in situ stain, Short-130 reversed monocrotaline-mediated changes in target genes Pparγ and Lrp8, decreased collagen deposition and remodeling (Picrosirius Red), and medial thickening (α-SMA). In turn, Yap nuclear localization decreased. (B) qRT-PCR demonstrated a decrease in fibrillar collagen isoforms, Lox, and Ctgf in Short-130-treated lung. (C) Short-130 decreased Lox activity in PH lung. (D) Short-130 decreased monocrotaline-induced collagen deposition (left) and fibrillar collagen content (right) in PH lung. (E) Co-immunofluorescence microscopy revealed YAP-positive proliferating cells (PCNA/YAP double-positive stain) in diseased pulmonary arterioles (Short-NC). Short-130 reduced the number of PCNA/YAP double-positive cells in $CD31^+$ and $CD31^-$ compartments. (F and G) Short-130 decreased the miR-130/301-mediated increase in PH severity, as quantified by RVSP (F) and right ventricular hypertrophy (G).

(H and I) After 2 weeks of PH induction with hypoxia + SU5416, mice were serially injected with Short-NC or Short-130 along with hypoxia + SU5416 for 2 more weeks. Short-130 decreased collagen deposition and fibrillar collagen (Picrosirius Red) (H). Atomic force microscopy revealed increased pulmonary arteriolar (<50 μm) stiffness in PH, but Short-130 blunted this alteration (I). Black lines denote median; symbols denote individual PA measurements (n = 4 normoxic mice versus n = 3/hypoxic group). p values were calculated by Kruskal-Wallis testing followed by Mann Whitney *U* post hoc analysis; a significance cutoff of < 0.008 was based on Bonferroni correction.

(J) Transcriptomic analyses of whole mouse lung were performed after exposure to hypoxia + SU5416 treated with Short-NC (n = 3) or Short-130 (n = 3) versus mice in normoxia + SU5416 (control; n = 3). Genes from this transcriptomic analysis were identified according to modulation by both hypoxia and miR-130/301 inhibition. Pathway enrichment identified ECM modification as the pathway with the lowest hypergeometric p value. Genes are color-coded according to membership in the five pathways with lowest p values. Enlarged genes are shared by the fibrosis network (see Figure 2A).

Data are expressed as mean ± SEM (*p < 0.05; **p < 0.01). Scale bars, 50 μm. See also Figure S5.

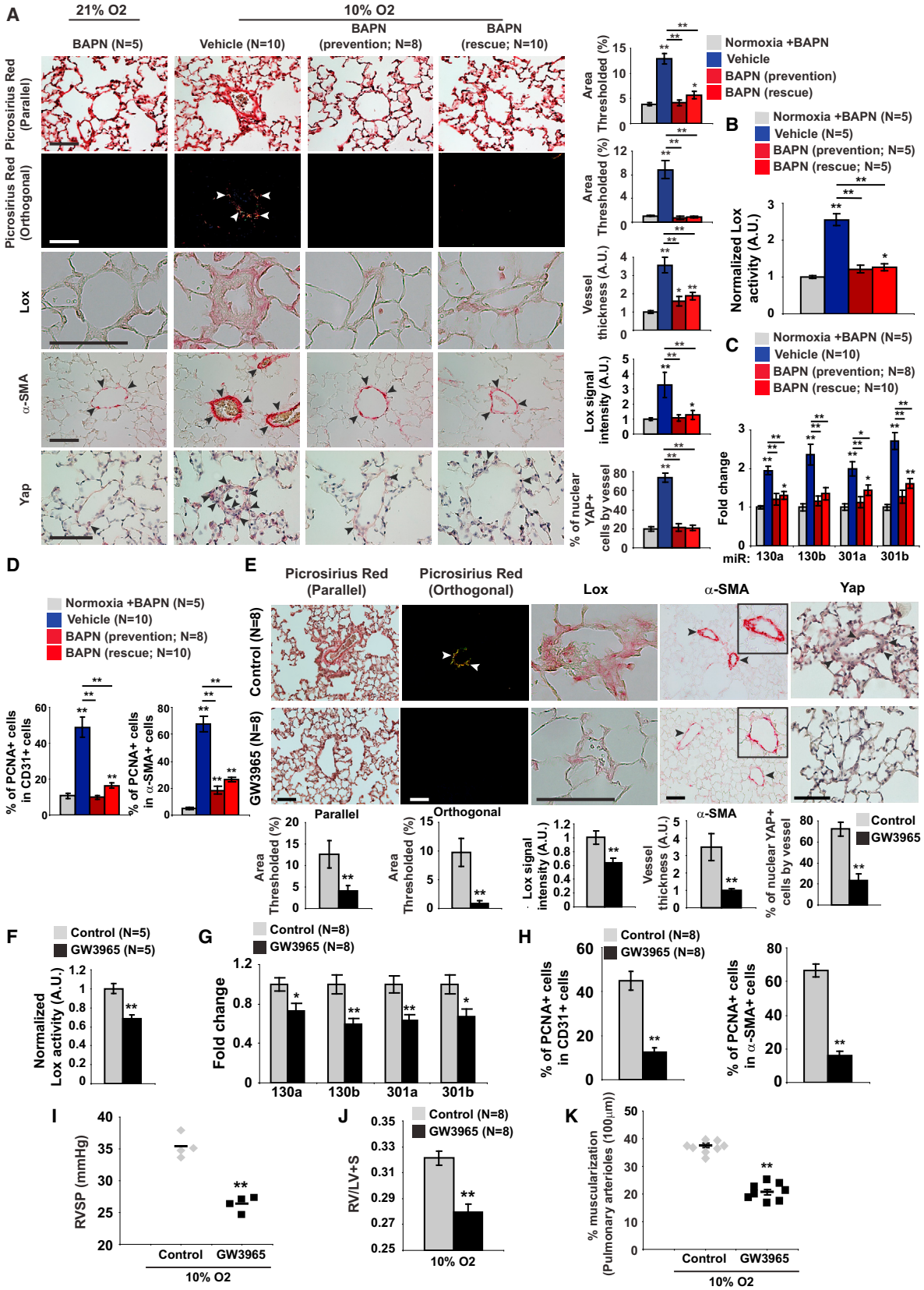

(legend on next page)

and downstream cellular crosstalk. Coupled with the feasibility of therapeutically manipulating multiple targets in this pathway, these results support the application of cooperative therapeutic maneuvers that ameliorate vascular stiffness and thus prevent or reverse multiple forms of human PH.

EXPERIMENTAL PROCEDURES

Study Approval

All animal experiments were approved by the Harvard Center for Comparative Medicine, the University of Colorado, Denver, and the Committees on Animal Research of the University of California, San Francisco. All experimental procedures involving the use of human tissue were approved by institutional review boards at Partners Healthcare, Boston Children's Hospital, and University of California, Los Angeles, as well as the New England Organ Bank. Ethical approval for this study and informed consent conformed to the standards of the Declaration of Helsinki. For formalin-fixed paraffin-embedded lung samples, human PH specimens from unused or discarded surgical samples and non-diseased human lung specimens from the New England Organ Bank have been described (Bertero et al., 2014).

Oligonucleotides and Transfection

Pre-miRNA oligonucleotides (pre-miR-130a, negative control pre-miR-NC1, and premiR-NC2) and custom-designed tiny LNA oligonucleotides (tiny-130: 5′-ATTGCACT-3′ and tiny-NC: 5′-TCATACTA-3′) were purchased from Thermo Scientific/Ambion and Exiqon, respectively. siRNAs for PPARγ (sc-29455), OCT4/POU5F1 (sc-5279), and scrambled control (sc-44236) were purchased from Santa Cruz Biotechnology. On Target Plus siRNAs for YAP (J-012200-07), TAZ (WWTR1) (J-016083-05), LRP8 (J-011802-05), and scrambled control (D-001810-01) were purchased from Dharmacon (GE Healthcare). PAAFs, PAECs, and PASMCs were plated in collagen-coated plastic (50 μg/ml) and transfected 24 hr later at 70%–80% confluence using pre-miRNA (5 nM), tiny-LNA (20 nM), or siRNA (25 nM) and Lipofectamine 2000 reagent (Thermo Scientific), according to the manufacturer's instructions. Eight hours after transfection, cells were trypsinized and re-plated in hydrogel. Key siRNA experiments were replicated with a second independent siRNA sequence targeting YAP (J-012200-05, Dharmacon), TAZ (J-016083-06, Dharmacon), PPARγ (sc-44220, Santa Cruz Biotechnology), and LRP8 (J-011802-06, Dharmacon) as well as scrambled controls (sc-37007 Santa Cruz Biotechnology and D-001810-02 Dharmacon).

Forced Pulmonary Expression of miR-130a in Lungs of Mice In Vivo

Eight-week-old mice (C57Bl6) were injected with SU5416 (20 mg/kg; Sigma-Aldrich), followed by four intrapharyngeal injections (once per week) of 1 nmol miR-control (pre-miR-NC) or miR-130a (pre-miR-130a) mixed in 100 μl PBS solution containing 5% Lipofectamine 2000 (Thermo Scientific). Such intrapharyngeal injections led to effective delivery to the pulmonary arterioles, as we previously described in detail (Bertero et al., 2014). BAPN (Sigma-Aldrich) was dissolved in water and administered daily in indicated mouse cohorts (30 mg/kg/day). Three days after the last oligonucleotide injection, right heart catheterization was performed as previously described (Parikh et al., 2012), followed by harvest of lung tissue for RNA extraction or paraffin embedding, as described above.

Inhibition of miR-130/301 in a Rat Model of Monocrotaline-Induced PH

Male Sprague-Dawley rats (10–14 weeks old) were injected with 60 mg/kg monocrotaline at time 0 followed by five intraperitoneal injections (every 3 days) of control or miR-130/301 shortmer oligonucleotides (20 mg/kg/dose; Regulus). Three days after the last injection, right heart catheterization was performed followed by harvest of lung tissue for RNA extraction or paraffin embedding.

Inhibition of miR-130/301 in a Mouse Model of PH

Eight-week-old mice (C57Bl6) were injected with SU5416 (20 mg/kg/dose/week; Sigma-Aldrich), followed by exposure to normobaric hypoxia (10% O_2; OxyCycler chamber, Biospherix Ltd, Redfield, NY) for 2 weeks. After 2 weeks and confirmation of PH development in five mice (right heart catheterization), mice were further treated with hypoxia + SU5416, along with three intrapharyngeal injections (every 4 days) of control or miR-130/301 shortmer oligonucleotides, designed as fully modified antisense oligonucleotides complementary to the seed sequence of the miR-130/301 miRNA family (10 mg/kg; Regulus). Specifically, the control and miR-130/301 shortmer oligonucleotides were non-toxic, lipid-permeable, high-affinity oligonucleotides. The miR-130/301 shortmer carried a sequence complementary to the active site of the miR-130/301 miRNA family, containing a phosphorothioate backbone and modifications (fluoro, methoxyethyl, and bicyclic sugar) at the sugar 2′ position. Such intrapharyngeal injections led to effective delivery to the pulmonary arterioles, as we previously described in detail (Bertero et al., 2014). Three days after the last injection, right heart catheterization was performed followed by harvest of lung tissue for RNA extraction or paraffin embedding, as described above.

Treatment of Hypoxic Mice with BAPN

Mice were exposed to normoxia or chronic hypoxia, and treated with BAPN (Sigma-Aldrich, 30 mg/kg/day as described above) or vehicle control, either simultaneously with hypoxia ("prevention") or after disease development ("reversal") (Figure S6A). Specifically, normoxic mice and hypoxic mice were treated either with BAPN or vehicle for 4 weeks ("prevention"). Alternatively, mice were exposed to hypoxia for 2 weeks to induce PH and then treated with BAPN along with 2 more weeks of hypoxic exposure ("reversal"). After these time periods, right heart catheterization was performed followed by harvest of lung tissue for RNA extraction or paraffin embedding.

Treatment of Hypoxic Mice with Oral Ingestion of the Liver-X Nuclear Hormone Receptor Agonist GW3965

To determine the effects of the LXR agonist GW3965 (Sigma-Aldrich) and consequent APOE induction on PH development, as previously described (Pencheva et al., 2014), mice were exposed to normobaric hypoxia and simultaneously assigned to control chow or chow supplemented with GW3965 (Research Diets) at doses of 100 mg drug per kilogram mouse per day (based on average daily intake of 3.5 g chow). After 3 weeks, right heart

Figure 7. Pharmacologic Inhibition of LOX or Activation of APOE Disrupts YAP/TAZ-miR-130/301 Signaling to Reduce Vascular ECM Remodeling and PH

(A–D) Mice were treated with BAPN either simultaneously with hypoxia (prevention) or after hypoxic disease induction (reversal). In prevention and rescue experiments, BAPN blunted hypoxia-mediated increases of vascular Lox, collagen remodeling (Picrosirius Red), medial thickening (α-SMA) (A), and Lox activity (B). In correlation with these ECM modifications, BAPN decreased Yap nuclear localization (A), miR-130/301 (C), and proliferation (PCNA positive) of arteriolar $CD31^+$ and α-SMA+ cells as compared with diseased controls (D).

(E–K) Hypoxic mice were treated with the LXR agonist GW3965 by prevention protocol. Similar to BAPN, the LXR agonist GW3965 blunted hypoxia-mediated increases of Lox, collagen remodeling (Picrosirius Red), medial thickening (α-SMA) (E), and Lox activity (F). Consistent with such ECM alterations, GW3965 decreased Yap nuclear localization (E), miR-130/301 (G), and downstream pulmonary vascular proliferation (PCNA stain in arteriolar $CD31^+$ and α-SMA+ cells) compared with diseased controls (H). Consequently, GW3965 ameliorated PH severity, as quantified by RVSP (I), right ventricular hypertrophy (Fulton index, RV/LV+S) (J), and arteriolar muscularization (K).

Data are expressed as mean ± SEM (*$p < 0.05$; **$p < 0.01$). Normalized values are expressed as arbitrary units (A.U.) in (A), (B), (E), and (F). Scale bars 50 μm. See also Figure S6.

catheterization was performed followed by harvest of lung tissue for RNA extraction or paraffin embedding.

Statistics

Cell culture experiments were performed at least three times and at least in triplicate for each replicate. The number of animals in each group was calculated to measure at least a 20% difference between the means of experimental and control groups with a power of 80% and an SD of 10%. The number of unique patient samples for this study was determined primarily by clinical availability. In situ expression/histologic analyses of both rodent and human tissue, and pulmonary vascular hemodynamics in mice and rats were performed in a blinded fashion. Numerical quantifications for in vitro experiments using cultured cells or in situ quantifications of transcript/miRNA expression represent mean ± SD. Numerical quantifications for physiologic experiments using rodents or human reagents represent mean ± SEM. Immunoblot images are representative of experiments that have been repeated at least three times. Micrographs are representative of experiments in each relevant cohort. Unless otherwise stated, paired samples were compared by a two-tailed Student's t test, and multiple group comparisons were performed by one-way ANOVA and post hoc Bonferroni testing. For comparison among non-normally distributed data (i.e., atomic force microscopy data), a Mann-Whitney *U* test was used for paired samples. For multiple comparisons in Figure 6I, Kruskal-Wallis testing was followed by post hoc between-group Mann Whitney *U* tests. Of note, for such multiple comparisons, we utilized a p value significance cutoff of <0.008, based on a Bonferroni correction of p (0.05) for the number of comparisons (six) among these four cohorts of mice. Otherwise, a p value < 0.05 was considered significant. Correlation analyses were performed by Pearson correlation coefficient calculation.

Please see Supplemental Experimental Procedures for further details of standardized and/or previously described methods and reagents.

ACCESSION NUMBERS

The accession number for the RNA-seq experimental data and associated designs is GEO: GSE61828.

SUPPLEMENTAL INFORMATION

Supplemental information includes Supplemental Experimental Procedures, six figures, and six tables and can be found with this article online at http://dx.doi.org/10.1016/j.celrep.2015.09.049.

AUTHOR CONTRIBUTIONS

T.B., K.A.C., and S.Y.C. conceived and designed the experiments. K.A.C. and V.K. performed the in silico analyses. T.B., Y.L., C.M.H., P.D., S.A., A.H., Y.-Y.Z., and L.E.F. performed the experiments. B.B.G., R.K., R.S., R.S., W.D.W., D.J.R., S.M.B., S.F., J.R.F., S.O.V., K.J.H., and A.B.W. performed the work to obtain human and animal PH reagents. B.B. and B.N.C. constructed the anti-miR reagents. T.B., K.A.C., C.M.H., P.D., L.E.F., and S.Y.C. wrote the manuscript. All authors participated in interpreting the results and revising the manuscript.

ACKNOWLEDGMENTS

We thank J. Androsavich for technical assistance. This work was supported by the NIH grants HL096834 and HL124021 to S.Y.C., HL67841 to S.M.B., and HL61284 to J.R.F.); the McArthur-Radovsky, Lerner, Harris, and Watkins Funds (S.Y.C.); the Pulmonary Hypertension Association (S.Y.C.); the American Heart Association (postdoctoral award, T.B.); and Foundation Bettencourt-Schueller (T.B.).

Received: January 26, 2015
Revised: August 7, 2015
Accepted: September 17, 2015
Published: October 22, 2015

REFERENCES

Bertero, T., Lu, Y., Annis, S., Hale, A., Bhatt, B., Saggar, R., Saggar, R., Wallace, W.D., Ross, D.J., Vargas, S.O., et al. (2014). Systems-level regulation of microRNA networks by miR-130/301 promotes pulmonary hypertension. J. Clin. Invest. *124*, 3514–3528.

Bertero, T., Cottrill, K., Krauszman, A., Lu, Y., Annis, S., Hale, A., Bhat, B., Waxman, A.B., Chau, B.N., Kuebler, W.M., and Chan, S.Y. (2015). The microRNA-130/301 family controls vasoconstriction in pulmonary hypertension. J. Biol. Chem. *290*, 2069–2085.

Bi, R., Bao, C., Jiang, L., Liu, H., Yang, Y., Mei, J., and Ding, F. (2015). MicroRNA-27b plays a role in pulmonary arterial hypertension by modulating peroxisome proliferator-activated receptor γ dependent Hsp90-eNOS signaling and nitric oxide production. Biochem. Biophys. Res. Commun. *460*, 469–475.

Boutet, K., Montani, D., Jaïs, X., Yaïci, A., Sitbon, O., Simonneau, G., and Humbert, M. (2008). Therapeutic advances in pulmonary arterial hypertension. Ther. Adv. Respir. Dis. *2*, 249–265.

Chan, S.Y., and Loscalzo, J. (2008). Pathogenic mechanisms of pulmonary arterial hypertension. J. Mol. Cell. Cardiol. *44*, 14–30.

Ciuclan, L., Bonneau, O., Hussey, M., Duggan, N., Holmes, A.M., Good, R., Stringer, R., Jones, P., Morrell, N.W., Jarai, G., et al. (2011). A novel murine model of severe pulmonary arterial hypertension. Am. J. Respir. Crit. Care Med. *184*, 1171–1182.

Cowan, K.N., Heilbut, A., Humpl, T., Lam, C., Ito, S., and Rabinovitch, M. (2000). Complete reversal of fatal pulmonary hypertension in rats by a serine elastase inhibitor. Nat. Med. *6*, 698–702.

Dufort, C.C., Paszek, M.J., and Weaver, V.M. (2011). Balancing forces: architectural control of mechanotransduction. Nat. Rev. Mol. Cell Biol. *12*, 308–319.

Dupont, S., Morsut, L., Aragona, M., Enzo, E., Giulitti, S., Cordenonsi, M., Zanconato, F., Le Digabel, J., Forcato, M., Bicciato, S., et al. (2011). Role of YAP/TAZ in mechanotransduction. Nature *474*, 179–183.

Friedman, R.C., Farh, K.K., Burge, C.B., and Bartel, D.P. (2009). Most mammalian mRNAs are conserved targets of microRNAs. Genome Res. *19*, 92–105.

Gan, C.T., Lankhaar, J.W., Westerhof, N., Marcus, J.T., Becker, A., Twisk, J.W., Boonstra, A., Postmus, P.E., and Vonk-Noordegraaf, A. (2007). Noninvasively assessed pulmonary artery stiffness predicts mortality in pulmonary arterial hypertension. Chest *132*, 1906–1912.

Hansmann, G., de Jesus Perez, V.A., Alastalo, T.P., Alvira, C.M., Guignabert, C., Bekker, J.M., Schellong, S., Urashima, T., Wang, L., Morrell, N.W., and Rabinovitch, M. (2008). An antiproliferative BMP-2/PPARgamma/apoE axis in human and murine SMCs and its role in pulmonary hypertension. J. Clin. Invest. *118*, 1846–1857.

Huang, Y., He, Y., and Li, J. (2015). MicroRNA-21: a central regulator of fibrotic diseases via various targets. Curr. Pharm. Des. *21*, 2236–2242.

Im, S.S., and Osborne, T.F. (2011). Liver x receptors in atherosclerosis and inflammation. Circ. Res. *108*, 996–1001.

Kerr, J.S., Riley, D.J., Frank, M.M., Trelstad, R.L., and Frankel, H.M. (1984). Reduction of chronic hypoxic pulmonary hypertension in the rat by beta-aminopropionitrile. J. Appl. Physiol. *57*, 1760–1766.

Kerr, J.S., Ruppert, C.L., Tozzi, C.A., Neubauer, J.A., Frankel, H.M., Yu, S.Y., and Riley, D.J. (1987). Reduction of chronic hypoxic pulmonary hypertension in the rat by an inhibitor of collagen production. Am. Rev. Respir. Dis. *135*, 300–306.

Kim, K.M., Choi, Y.J., Hwang, J.H., Kim, A.R., Cho, H.J., Hwang, E.S., Park, J.Y., Lee, S.H., and Hong, J.H. (2014). Shear stress induced by an interstitial level of slow flow increases the osteogenic differentiation of mesenchymal stem cells through TAZ activation. PLoS ONE *9*, e92427.

Kothapalli, D., Liu, S.L., Bae, Y.H., Monslow, J., Xu, T., Hawthorne, E.A., Byfield, F.J., Castagnino, P., Rao, S., Rader, D.J., et al. (2012). Cardiovascular protection by ApoE and ApoE-HDL linked to suppression of ECM gene expression and arterial stiffening. Cell Rep. *2*, 1259–1271.

Lammers, S., Scott, D., Hunter, K., Tan, W., Shandas, R., and Stenmark, K.R. (2012). Mechanics and Function of the Pulmonary Vasculature: Implications for Pulmonary Vascular Disease and Right Ventricular Function. Compr. Physiol. *2*, 295–319.

Levental, K.R., Yu, H., Kass, L., Lakins, J.N., Egeblad, M., Erler, J.T., Fong, S.F., Csiszar, K., Giaccia, A., Weninger, W., et al. (2009). Matrix crosslinking forces tumor progression by enhancing integrin signaling. Cell *139*, 891–906.

Lian, I., Kim, J., Okazawa, H., Zhao, J., Zhao, B., Yu, J., Chinnaiyan, A., Israel, M.A., Goldstein, L.S., Abujarour, R., et al. (2010). The role of YAP transcription coactivator in regulating stem cell self-renewal and differentiation. Genes Dev. *24*, 1106–1118.

Liu, F., Lagares, D., Choi, K.M., Stopfer, L., Marinković, A., Vrbanac, V., Probst, C.K., Hiemer, S.E., Sisson, T.H., Horowitz, J.C., et al. (2015). Mechanosignaling through YAP and TAZ drives fibroblast activation and fibrosis. Am. J. Physiol. Lung Cell. Mol. Physiol. *308*, L344–L357.

Mecham, R.P., Whitehouse, L.A., Wrenn, D.S., Parks, W.C., Griffin, G.L., Senior, R.M., Crouch, E.C., Stenmark, K.R., and Voelkel, N.F. (1987). Smooth muscle-mediated connective tissue remodeling in pulmonary hypertension. Science *237*, 423–426.

Merklinger, S.L., Wagner, R.A., Spiekerkoetter, E., Hinek, A., Knutsen, R.H., Kabir, M.G., Desai, K., Hacker, S., Wang, L., Cann, G.M., et al. (2005). Increased fibulin-5 and elastin in S100A4/Mts1 mice with pulmonary hypertension. Circ. Res. *97*, 596–604.

Mouw, J.K., Yui, Y., Damiano, L., Bainer, R.O., Lakins, J.N., Acerbi, I., Ou, G., Wijekoon, A.C., Levental, K.R., Gilbert, P.M., et al. (2014). Tissue mechanics modulate microRNA-dependent PTEN expression to regulate malignant progression. Nat. Med. *20*, 360–367.

Nave, A.H., Mižíková, I., Niess, G., Steenbock, H., Reichenberger, F., Talavera, M.L., Veit, F., Herold, S., Mayer, K., Vadász, I., et al. (2014). Lysyl oxidases play a causal role in vascular remodeling in clinical and experimental pulmonary arterial hypertension. Arterioscler. Thromb. Vasc. Biol. *34*, 1446–1458.

Nickel, N.P., Spiekerkoetter, E., Gu, M., Li, C.G., Li, H., Kaschwich, M., Diebold, I., Hennigs, J.K., Kim, K.Y., Miyagawa, K., et al. (2015). Elafin reverses pulmonary hypertension via caveolin-1-dependent bone morphogenetic protein signaling. Am. J. Respir. Crit. Care Med. *191*, 1273–1286.

Parikh, V.N., Jin, R.C., Rabello, S., Gulbahce, N., White, K., Hale, A., Cottrill, K.A., Shaik, R.S., Waxman, A.B., Zhang, Y.Y., et al. (2012). MicroRNA-21 integrates pathogenic signaling to control pulmonary hypertension: results of a network bioinformatics approach. Circulation *125*, 1520–1532.

Pencheva, N., Buss, C.G., Posada, J., Merghoub, T., and Tavazoie, S.F. (2014). Broad-spectrum therapeutic suppression of metastatic melanoma through nuclear hormone receptor activation. Cell *156*, 986–1001.

Piccolo, S., Dupont, S., and Cordenonsi, M. (2014). The biology of YAP/TAZ: hippo signaling and beyond. Physiol. Rev. *94*, 1287–1312.

Poiani, G.J., Tozzi, C.A., Yohn, S.E., Pierce, R.A., Belsky, S.A., Berg, R.A., Yu, S.Y., Deak, S.B., and Riley, D.J. (1990). Collagen and elastin metabolism in hypertensive pulmonary arteries of rats. Circ. Res. *66*, 968–978.

Stenmark, K.R., and Rabinovitch, M. (2010). Emerging therapies for the treatment of pulmonary hypertension. Pediatr. Crit. Care Med. *11* (*2, Suppl*), S85–S90.

Valastyan, S., and Weinberg, R.A. (2011). Roles for microRNAs in the regulation of cell adhesion molecules. J. Cell Sci. *124*, 999–1006.

Wang, Z., and Chesler, N.C. (2011). Pulmonary vascular wall stiffness: An important contributor to the increased right ventricular afterload with pulmonary hypertension. Pulm. Circ. *1*, 212–223.

Wang, D., Zhang, H., Li, M., Frid, M.G., Flockton, A.R., McKeon, B.A., Yeager, M.E., Fini, M.A., Morrell, N.W., Pullamsetti, S.S., et al. (2014). MicroRNA-124 controls the proliferative, migratory, and inflammatory phenotype of pulmonary vascular fibroblasts. Circ. Res. *114*, 67–78.

Wei, J., Bhattacharyya, S., Jain, M., and Varga, J. (2012). Regulation of matrix remodeling by peroxisome proliferator-activated receptor-γ: a novel link between metabolism and fibrogenesis. Open Rheumatol. J. *6*, 103–115.

White, K., Loscalzo, J., and Chan, S.Y. (2012). Holding our breath: The emerging and anticipated roles of microRNA in pulmonary hypertension. Pulm. Circ. *2*, 278–290.

Zhou, J. (2014). An emerging role for Hippo-YAP signaling in cardiovascular development. J. Biomed. Res. *28*, 251–254.

Zhou, Z., Hu, T., Xu, Z., Lin, Z., Zhang, Z., Feng, T., Zhu, L., Rong, Y., Shen, H., Luk, J.M., et al. (2015). Targeting Hippo pathway by specific interruption of YAP-TEAD interaction using cyclic YAP-like peptides. FASEB J. *29*, 724–732.